Journal of The Electrochemical Society, **159** (4) H444-H449 (2012)
0013-4651/2012/159(4)/H444/6/$28.00 © The Electrochemical Society

$CuInSe_2$ (CIS) Thin Film Solar Cells by Electrostatic Spray Deposition

Hyun Yoon,[a] Ji Hoon Woo,[a] Bhavana Joshi,[a] Young Min Ra,[a] Sam S. Yoon,[a,z] Ho Young Kim,[a] SeJin Ahn,[b] Jae Ho Yun,[b] Jihye Gwak,[b] KyungHoon Yoon,[b] and Scott C. James[c]

[a]*School of Mechnical Engineering, Korea University, Anam-Dong, Seongbuk-Gu, Seoul, 136-713, Korea*
[b]*Photovoltaic Research Center, Korea Institute of Energy Research, Yuseong-Gu, Dae-Jeon, 305-343, Korea*
[c]*Thermal/Fluid Science & Engineering, Sandia National Laboratories, Livermore, California 94551, USA*

In this paper, we demonstrate, for the first time, the manufacture of a $CuInSe_2$ thin film whose absorber layer is coated using an electrostatic spray deposition (ESD) technique; its complete transformation into a working device with measured conversion efficiency is presented. ESD is superior to pneumatic spraying because it produces nano-scaled, self-dispersive (non-agglomerating), highly wettable (electrowetting) and adhesive droplets to yield a uniform coating on a substrate. Furthermore, ESD's extremely low material consumption rate holds promises for practical use in the solar cell industry. Copper and indium salts are added to various solvents, which are electrostatically sprayed onto a molybdenum-coated soda-lime glass substrate. The effect of substrate temperature on the thin film characteristics is examined. Our cell is completed by adding CdS and ZnO layers onto the $CuInSe_2$ absorber layer. Light illuminated current-density voltage (*J-V*) characteristics demonstrate a power conversion efficiency of $\eta = 1.75\% \pm 0.09$ with an open-circuit voltage of $V_{OC} = 0.23$ V, a short-circuit current density of $J_{SC} = 21.72$ mA/cm^2, and fill factor of $FF = 0.34$.
 [DOI: 10.1149/2.jes113086]

Manuscript received October 31, 2011. Published February 7, 2012.

Manufacturability of thin films is more flexible than c-Si solar cells because thin films can be deposited both by vacuum (i.e., co-evaporation, sputtering, PECVD) and non-vacuum methods (i.e., spray pyrolysis, electrodeposition, electroless deposition, chemical bath deposition, doctor blading, and pasting). Versatile choices for the substrate further enhance the merits of thin films; substrate choices include glass, flexible polymer sheets, and flexible stainless steel. General advantages of thin films are: (1) minimized material consumption, (2) low-cost substrate availability (e.g., soda-lime glass, stainless steel, foil, and polymers), (3) availability of flexible, light, strong, and thin substrates that are resistant to degradation by solar radiation and severe environments.

Among common thin films (e.g., amorphous silicon, a-Si, cadmium telluride, CdTe, gallium arsenide, GaAs, CIS-based, or CuIn(Ga)Se), CIS-based thin films are the most promising candidates to improve cost competitiveness. CIS-based solar cells are attractive because of: (1) favorable optical and electrical properties such as tunable band gaps from 1 to 2.4 eV through addition of gallium (Ga) and sulfur (S) that capture shorter light wavelengths, (2) large photon absorption coefficients, and (3) relatively high power-conversion efficiencies.[1] However, advances in CIS-based solar cells have been hampered by high manufacturing costs and the capital and energy requirements of conventional vacuum deposition methods (e.g., co-evaporation and sputtering). Non-vacuum-based deposition methods would greatly reduce costs and enhance solar-energy-technology market penetration.

Non-vacuum methods include spin-coating, electro-deposition, screen-printing, doctor-blading, paste-coating, printing-precursor, and spray pyrolysis.[2] Mitzi[2–4] and Milliron et al.[5] used non-vacuum spin coating to deposit a Cu-In-Ga-Se (CIGS) precursor (using a hydrazine solvent) and achieved a power conversion efficiency of 10.3%. Such efficiency was possible because hydrazine dissolves binary chalcogenides, such as Cu-S, In-Se, Ga-Se, without any additives; hence, it precludes impurities such as carbon and oxygen that increase the resistance of the film and hinder solar cell performance.[2,6] However, the reactivity and toxicity of hydrazine limit widespread use. Ahn et al.[7] coated a substrate with Cu-In solutions (i.e., $Cu(NO_3)_2$ and $InCl_3$, which are non-toxic, relatively safe, and inexpensive) using the doctor-blading technique, but achieved a low efficiency of 2% because of impurities, especially from the ethyl-cellulose solvent, which is a highly viscous additive required to spread the precursor without dripping. Spraying has also received attention as a layer coating technique because of its rapidity and ability to cover large areas.[8] Previous spraying studies in relation to the solution-based approach are summarized in Table I. Tomar and Garcia[9] demonstrated a 2% conversion efficiency with a spray-coated thin film solar cell of $ZnO/CuInSe_2$ heterojunction. Bougnot et al.[10] also sprayed precursors containing $CuCl_2$, $InCl_3$, and N-dimethyl selenourea mixed with ethanol and deionized water; a good chalcopyrite structure with a strong (112)-oriented thin film was obtained; no conversion efficiency was reported. Raja-Ram et al.[11] reported a conversion efficiency of 3.15% for $CdZnS/CuInSe_2$ cells with aqueous solutions of $CdCl_2$, $ZnCl_2$, and $InCl_3$ for the CdZnS buffer layer, and $CuCl_2$, $InCl_3$, and selenourea for the $CuInSe_2$ absorber layer. Shirakata et al.[12] also used a similar aqueous precursor to produce a $CuInSe_2$ film; no conversion efficiency was reported.

Our approach is slightly different from the aforementioned approaches. We take the aqueous- or solution-based approach because, in general, particle-based approaches require complicated syntheses of nanocrystals (or powders or alloys), which generally suffer from low yield, poor crystallinity, and poor uniformity in composition and phase due to the complexity of the compounds at the nanometer scale.[7,13] By avoiding the complexities associated with particle-based approaches in favor of a solution-based approach, the cost competitiveness of non-vacuum spraying methods may improve.

Because copper and indium salts, but not selenium, are added to our solvent, this spray pyrolysis technique requires a high-temperature post-selenization process to make a solar cell. While this adds an additional step to the process (which increases production costs), it simplifies management of toxic selenium vapor because it is absent in the Cu-In precursor. Here, *solvent* refers to the dissolving liquid prior to its mixing with Cu and In, while the *precursor* refers to the final spraying liquid that contains Cu and In.

Instead of conventional pneumatic spraying, an electrostatic spray deposition technique (ESD) is used in this effort. ESD is superior to pneumatic spraying because it produces extremely fine (sub-micron), self-dispersive (non-agglomerating), highly wettable (electrowetting) and adhesive droplets to yield a uniform coating on the substrate; see Fig. 1a. In addition, because charged droplets are accelerated toward the substrate, targeting is improved resulting in high deposition efficiency. Certainly, several researchers have produced thin films for solar applications using ESD;[14–16] however, cell conversion efficiency has never been reported.

[z] E-mail: skyoon@korea.ac.kr

Table I. Previous studies on $CuInSe_2$ solar cell device produced by spraying solution-based precursors.

Previous Studies	Solvent	Nature of substrate	Substrate temperature	Conversion efficiency
Bougnot et al. (1986)	Ethanol Deionized water	Pyrex	180−200°C < 310°C	N.A.
Shirakata et al. (1996)	Ethanol	Stainless Steel	300−360°C	N.A.
Tomar and Garcia (1982)	Water, Ethanol	Pyrex, quartz	350−550°C	2%
Raja-Ram et al. (1986)	1,2-propanediol	Glass	300°C	3.15%

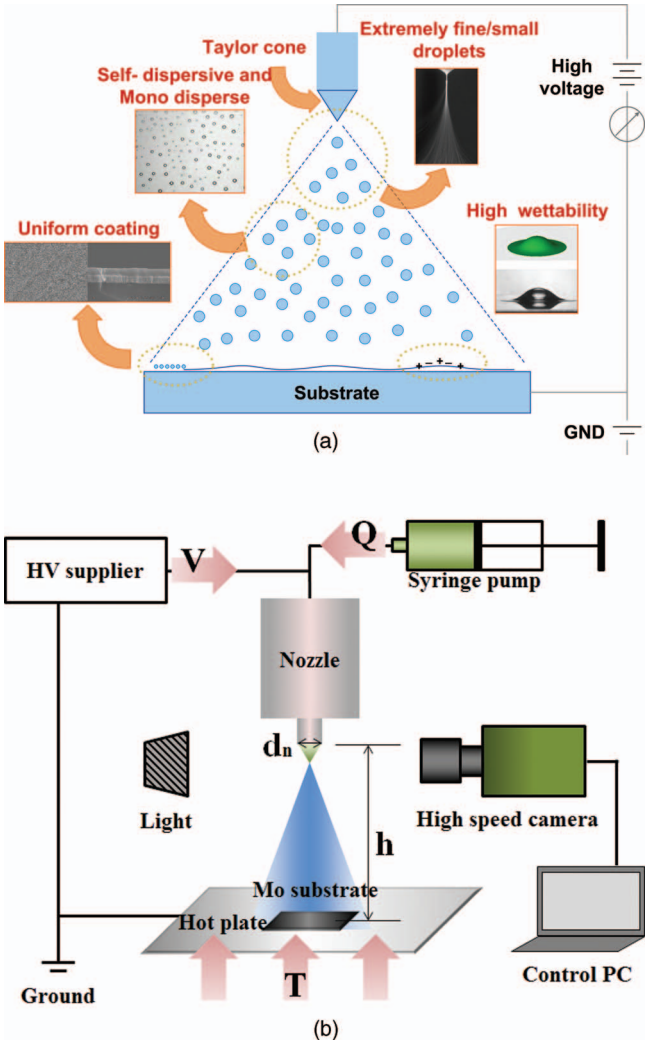

Figure 1. (a) Advantages of the electrostatic spray deposition thin-film coating technique. (b) Schematic of the ESD setup.

In this paper, we demonstrate, for the first time, the manufacture of a $CuInSe_2$ thin film whose absorber layer is prepared by ESD; it undergoes complete transformation into a working device with measured conversion efficiency. Various concentrations of the Cu-In precursor are examined. Optimized precursor flowrates, which vary with the thermo-electrical properties of the dissolving solvents, are also reported. The effect of substrate temperature on the thin films is also examined. The deposition operating conditions that yield the most uniform layer would be used to produce cells for the post-selenization process. Our cells are completed by adding CdS and ZnO layers onto the $CuInSe_2$ absorber layer. Finally, the current-voltage characteristics of the solar cell are presented.

Experimental Setup

Precursor preparation.— Inexpensive and non-toxic Cu-In salts are dissolved in alcohol-based solvents; all preparations are formulated at room temperature in air. The working fluids (solvents) are pure ethanol, butyl-carbitol, and propylene glycol. Copper nitrate hydrate ($Cu(NO_3)_2 \cdot 3H_2O$; 99.999%) and indium chloride ($InCl_3$; 99.999%) were purchased from *Sigma Aldrich*, and butyl-carbitol ($C_4H_9(OCH_2CH_2)_2OH$; 99.0%) and propylene glycol ($C_3H_8O_2$; 99.0%) from *Duksan Chemical*. Physical-chemical properties of the solvents are listed in Table II.

For precursors, the standard component ratio of Cu:In is 9:10 (i.e., Cu/In = 0.9). This copper-poor precursor is preferred because the conversion efficiency is maximized when the chalcopyrite grain structure with (112) orientation is formed.[10,17–21] The concentration of the precursor is varied by factors of 0.5 and 4 from the standard mixture concentration to investigate how this affects Cu-In content in the films; see snapshots of the precursors used in Fig. 2; the corresponding variation of K, γ, and μ is listed in Table III. A thicker film is required if the salt concentration is low and for absorber layer in solar cell an optimal thickness of 1 μm is needed after the post selenization process. The SEM images shown in Fig. 2c clearly reveal that ~1 μm thickness can be obtained at precursor concentration of ×4 in PG.

ESD spraying system.— The ESD system setup is shown in Fig. 1b. The downward-facing nozzle center is aligned with the plate center separated by a 45 mm gap with a spray diverging angle of 40°, which deposits the precursor onto an area of 25 mm × 25 mm on the Mo substrate. Molybdenum substrates provide the best back-contact (or electrode) performance because of their superior electrical conductivity and interfacial adhesion between the CIGS absorber layer and the electrode.[22] An ITO or fluorine tin oxide (FTO) substrate could have been used, but these have shown poorer performance for CIGS

Table II. Solvent and precursor physico-chemical properties.

Solvent	Q (mL/hr)	γ (mPa-s)	μ (mN/m)	ρ (g/cm^3)	K (μS/cm)	Boiling point (°C)
Ethanol	23	1.2	20.7	0.789	1.2	78
Ethanol w/ Cu-In	1	2.1	21.48	0.913	2124	Unknown
Butyl-carbitol	5	5.0	28.24	0.955	0.1	231
Butyl-carbitol w/ Cu-In	0.04	13.8	28.1	1.079	154.2	Unknown
Propylene glycol	18	37.30	40.1	1.036	10	188
Propylene glycol w/ Cu-In	0.04	34.8	83.4	1.084	378	Unknown

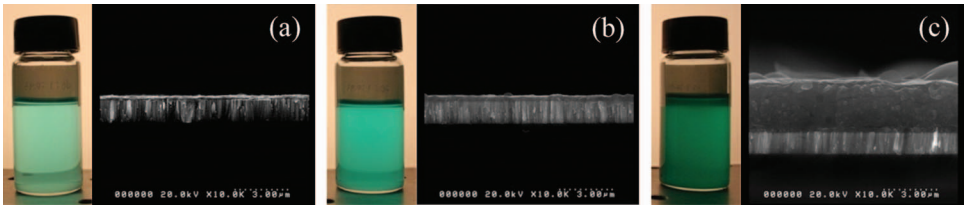

Figure 2. Snapshots of solution and SEM images of films at different Cu-In concentration in PG (a) ×0.5 (b) ×1.0 (c) ×4.0.

solar cells.[1] Furthermore, ITO and FTO may not withstand the high temperature requirements of the post-annealing selenization process.

The precursor issues from a syringe pump and the flowrate is adjusted to yield a stable Taylor cone, which produces the smallest droplets possible under the given operating conditions; see Fig. 3. The nozzle inner diameter is 3 mm. A voltage-supply wire is attached to the charging needle (i.e., anode) and the substrate is grounded (i.e., cathode). Precursor flowrates range from 0.02 to 5 mL/hr under applied voltages of 1 to 18 kV, yielding droplet sizes around a few hundred nanometers. Typically, it takes 10 to 15 minutes to yield a CIGS film of 1 to 2-μm thickness. While spraying Cu-In precursor, the Mo-substrate temperature is kept in the 100−200°C range to ensure pyrolysis and to form a solid thin film. The process parameters used for the deposited thin films are shown in Table IV.

Selenization.— Selenization was performed in a vacuum evaporator equipped with a Knudsen-type effusion cell. Initially the chamber was evacuated to a base pressure of 10^{-5} Torr with a turbo molecular pump and then elemental Se was evaporated from the effusion cell. Typical substrate temperature and selenization time were 530°C and 30 min, respectively. The flux of Se vapor was regulated by the effusion cell temperature.

Solar cell fabrication.— Solar cells were fabricated according to the conventional Mo/CIS/CdS/i-ZnO/n-ZnO/Al structure. In our baseline process, a 60-nm-thick CdS buffer layer was deposited onto the CIS film by chemical bath deposition and i-ZnO(50 nm)/Al-doped n-ZnO(500 nm) were deposited by radio-frequency magnetron sputtering on the CdS layer. A 500-nm-thick Al grid was deposited as a current collector, using thermal evaporation. The active area of a completed cell was 0.44 cm^2.

Thin film and device characterization.— The morphology, composition, and crystalline structure of the precursor films and the selenized films were investigated by high-resolution scanning electron microscopy (HRSEM, XL30SFEG Phillips Co., Holland at 10 kV), energy dispersive spectroscopy (EDS, EDAX Genesis apex, acceleration voltage: 30 kV; collection time: 100 s with a standardless method), and X-ray diffraction (XRD, Rigaku Japan, D/MAX-2500), using Cu KR-α line.

The compositional profile with depth of the selenized film was obtained by Auger electron spectroscopy (AES, Perkin-Elmer, SAM 4300). Device performances including the conversion efficiency and the EQE (external quantum efficiency) were measured with a class AAA solar simulator (WXS-155S-L2, WACOM, Japan).

Table III. Properties of the PG precursor.

Concentration	Electrical conductivity K (μS/cm)	Viscosity γ (mPa.s)	Surface tension μ (mN/m)
×0.5	185.7	34.6	64.2
×1.0	378	34.8	83.4
×4.0	426	35.9	156.9

Results and Discussion

Mass flowrate vs. conductivity.— Fig. 4a shows the effect of electrical conductivity ($K_{electrical}$) on the maximum flowrate, Q, that yields a stable Taylor cone subject to a 10 kV voltage. Ethanol (E) supports a higher stable flowrate than propylene glycol (PG) or butyl carbitol (BC) because of its lower viscosity. In general, the use of a higher viscosity solvent reduces the maximum flowrate of ESD.[23] Fig. 4a shows the flowrate as a function of electrical conductivity for each solvent during the cone-jet mode. Also shown in Fig. 4a is the maximum stable flowrate of ethanol as a function of conductivity, which was varied by adding nitric acid; ESD users should be particularly aware of this strong relationship (note the log scale for the y axis). Increasing conductivity decreases the maximum stable flowrate.[24] Highly conducting fluids have more ions at the cone surface that weaken surface tension (curvature) forces, resulting in thinner cone jets that prevent the precursor from efficient spraying; this is because $\kappa^{1/2}\gamma\varepsilon_0/\rho \sim Q_{min}K$ is constant, where κ is the dielectric constant (or relative permittivity), γ is the surface tension, Q is the flowrate, and ε_0 is the electrical permittivity in vacuum.[25,26] Basak et al.[27] developed scaling laws for particle diameters produced by drying droplets from electrospraying ionic precursors. They noted that the flowrate for the *strong* $Fe(NO_3)_3$ ionic (or electrolyte) precursor is 20–24 times less than the flowrate for the *weak* electrolyte. Because dissolved Cu-In salts increase precursor conductivity, higher concentrations will end up decreasing the maximum stable Taylor cone flowrate. While comparing the flowrates of ethanol, BC and PG with Cu-In, it is observed that the lower viscosity of ethanol makes it unsuitable for longer duration spraying because of its instability even if it allows higher flowrates. Therefore, the Cu-In films were deposited using only BC and PG

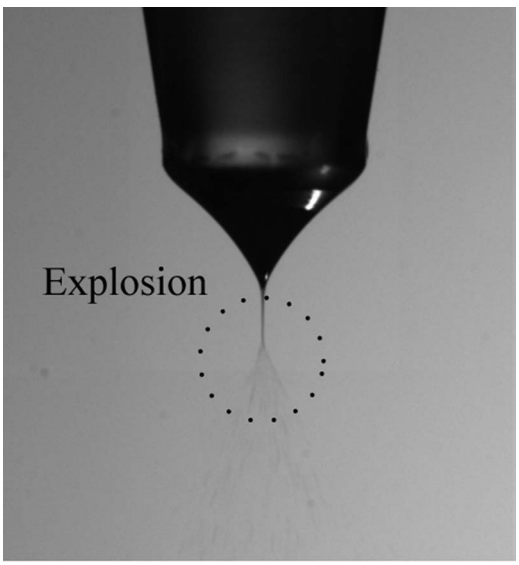

Figure 3. Spray generation from the Taylor cone, as a result of Rayleigh explosion.

Table IV. Process Parameters for Cu-In layer deposition.

Solvent	Flowrate (Q)	Voltage (V)	Nozzle diameter (d_n)	Separation distance (h)	Substrate temperature (T)
Butyl-carbitol	0.035–0.040 mL/hr	10 kV	30 mm	45 mm	150°C
Prorylene glycol		10 kV	30 mm	45 mm	100–200°C

solvent. The SEM image from Fig. 4b clearly shows that the surface morphology of the film deposited using the BC solvent is not uniform, as compare to the films obtained by using the PG-based solvents; see Fig. 5. Hence the absorber layer used for solar cell fabrication herein is deposited using the PG solvent with ×4 precursor concentration.

Precursor films.— The HR-SEM images in Fig. 5 show the morphologies of Cu-In films (PG solvent) deposited at substrate temperatures of (a) $T_{sub} = 100°C$ and (b) $T_{sub} = 200°C$. In the side views, the columnar structures are molybdenum, which is deposited onto the soda-lime glass by sputtering. Precursor films reside over the molybdenum layer. As indicated in the images, there are no voids in the precursor films. However, the surface morphology changes when the substrate temperature increases from 100 to 200°C. At $T_{sub} = 100°C$ in Fig. 5a, a clean, uniform, more crack-free film of less than 1 μm is obtained. At $T_{sub} = 200°C$ in Fig. 5b, a relatively irregular film is seen and the crack is found in the top view (left image). Because the hot substrate exceeds the boiling point of PG (186°C), the solvent quickly vaporizes from the precursor, often forming cracks in the thin film. Crack formation does not seem to be an issue because Cu-In films are mixed with selenium vapor during the post-selenization process and they tend to disappear, this phenomenon was confirmed in all of our tests. In general, higher substrate temperatures are desired to improve adhesion between the Mo-coated substrate and the Cu-In precursor and also to improve film crystallization. Nevertheless, in this study, we maintained a low substrate temperature because of the desire for low-temperature coating applications.

XRD analyzes of the precursor film (not shown here) indicate that copper is found in the form of CuCl (Cu^+). This may seem peculiar because $Cu(NO_3)_2$ was sprayed (Cu^{2+}), but Cu^{2+} was reduced to Cu^+ by accepting an electron from a reducing agent in the solvent mixture (e.g., propylene glycol reduces certain metallic ions). The EDS analysis showed that the atomic ratio of Cu and In varied from Cu/In = 0.8 to 1.0. XRD analyzes cannot detect the indium peak because indium does not exist in a crystalline state, but in an amorphous state. Chlorine content is not a significant issue because post-selenization vaporizes Cl_2 and precludes its inclusion in the film. In confirmation, Cl_2 was not detectable by EDS after the post-selenization process.

Fig. 6 shows a cross-sectional view of the precursor film deposited at $T_{sub} = 100°C$. At this low substrate temperature, the precursor is simply dried, rather than being pyrolyzed. Again, the PG precursor is used because of its stability during long duration of electro-spraying.[24] The film thickness is around 3.3 μm after 15 minutes of spraying. The precursor volume is estimated to be around $V_p = 0.002$ mL (i.e., 3.3 μm × 2.5 cm × 2.5 cm). Given the volumetric flowrate of 6.67×10^{-4} mL/min, it should take about 3 minutes to deposit the film assuming 100% deposition efficiency. However, because the spray is

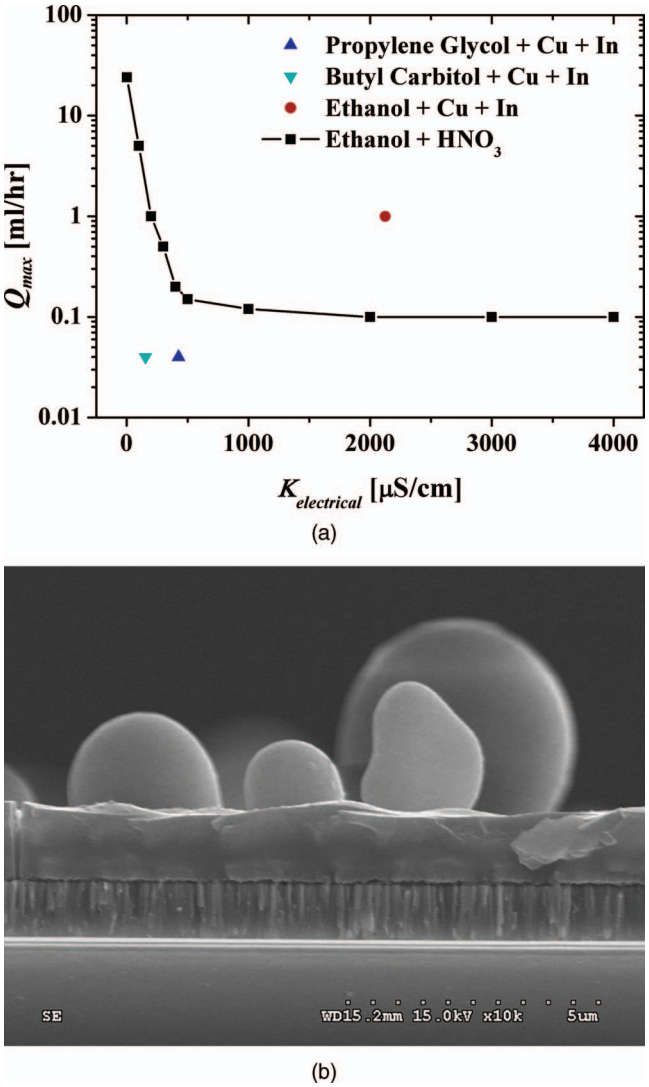

Figure 4. (a) Flowrate as a function of precursor electrical conductivity. As a reference, flowrates of ethanol with conductivity varied through addition of nitric acid are shown. (b) Cross sectional SEM image of BC solvent based Cu-In film showing nonuniform surface.

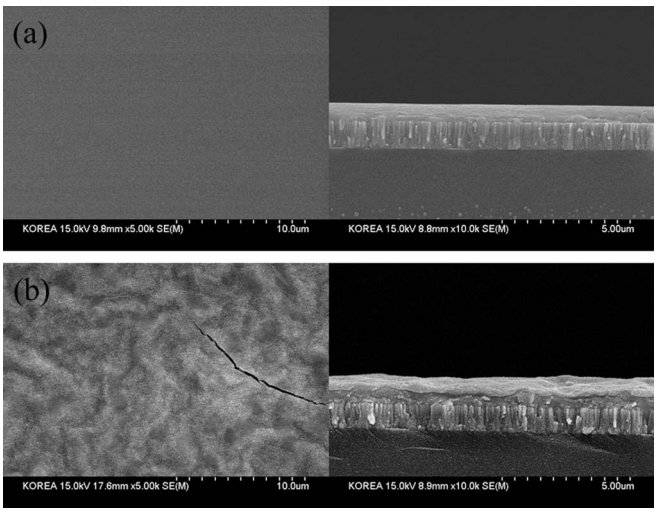

Figure 5. The morphologies of Cu-In films (PG solvent) deposited at substrate temperatures of (a) $T_{sub} = 100°C$ and (b) $T_{sub} = 200°C$. Left and right images are the top and side views, respectively.

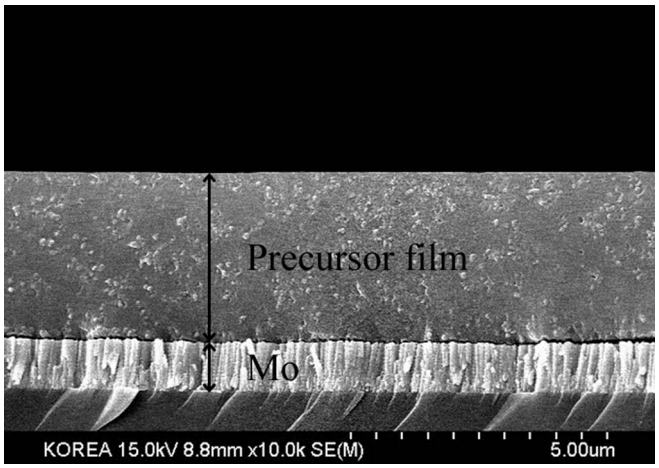

Figure 6. Cross-sectional SEM image of the substrate coated with the precursor film. The solvent is PG.

ejected in a diverging shape, there is some overspray outside the square cell that results in wasting precursors. Nevertheless, the deposition efficiency of our electro-spraying is notably superior to other pneumatic spraying methods. Other researchers reported flowrates in the range of 15–20 mL/min,[9,28] which is about 22,500 times greater than our flowrate, implying significant waste of precursor. Reduced spray rate and hence increased deposition efficiency is a notable advantage of the ESD technique.

Selenized films.— Fig. 7 shows SEM micrographs of the film after 30 minutes of selenization. Previous researchers have noted that In_2Se evaporation may result in excessive indium loss in the film during the selenization process.[29–31] To mitigate this possibility, a low selenization temperature and a high Se effusion cell temperature decrease the In_2Se evaporation rate by increasing the partial pressure of Se. However, the selenization temperature must be high enough to yield a chalcopyrite CIS film with a strong (112) orientation. Based on previous experience,[7] a selenization temperature of 530°C and a Se effusion cell temperature of 150°C are appropriately optimized to successfully crystallize the precursor film.

Fig. 7a is a top view of our well-crystallized dense $CuInSe_2$ film showing the flake-like structure of the film. Fig. 7b shows that the top $CuInSe_2$ film is about a half micron thick and it resides over an amorphous bottom layer whose thickness is also about a half micron. According to the XRD analysis in Fig. 8, the $CuInSe_2$ layer is indeed a chalcopyrite structure with a strong (112) preferred orientation. This indicates that the CuCl and amorphous In of the precursor are well crystallized into a $CuInSe_2$ film and that chlorine has been removed. The AES depth profile of the selenized film indicates more than 80% of the atomic percentage of the bottom layer is carbon. This carbon is considered impurity and is from the highly viscous PG solvent. While

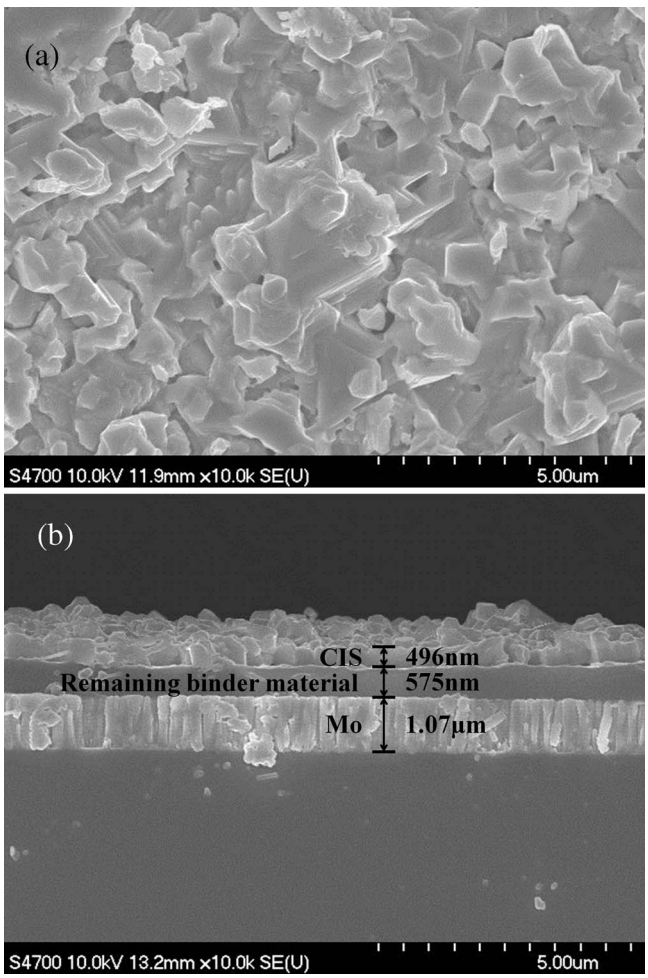

Figure 7. (a) Top and (b) side views of the selenized CIS thin film.

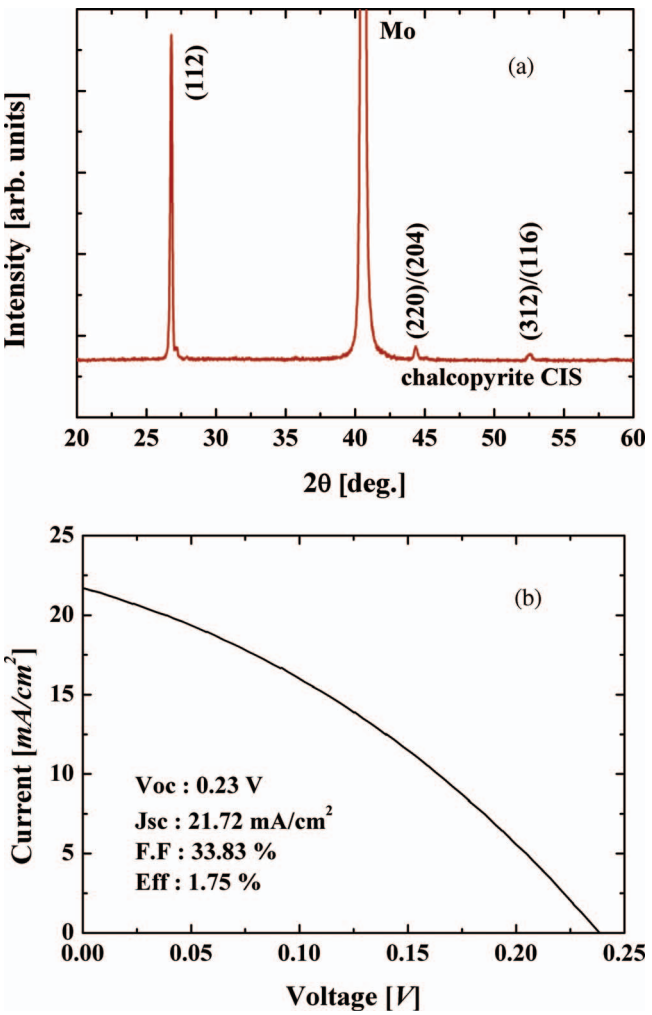

Figure 8. (a) The XRD pattern of the selenized sample in conjunction with Fig. 7. (b) I–V characteristics of the CIS solar cell on a molybdenum-coated substrate.

PG is easily evaporated at high temperatures in an open environment, once selenization begins, a $CuInSe_2$ layer begins to crystallize on top of it. At early stage of crystallization, PG finds pathways to evaporate, but ultimately, a $CuInSe_2$ canopy hinders any further evaporation of the PG. After complete selenization, there exists a CIS film atop the remaining precursor material; see the 0.575-μm-thick middle layer in Fig. 7b.

According to the EDS analysis, no Cl was observed in the selenized film. This indicates that the Cl^- from CuCl form Cl_2 gas during the selenization process and evaporated. A possible reaction route for $CuInSe_2$ film formation is suggested by:[7]

$$2CuCl_{(s)} + 2In - (Cl\,and/or\,NO_3)_{(s)} + 4Se_{(g)} \rightarrow 2CuInSe_{2(s)} + Cl_{2(g)} \uparrow \text{and/or} \, NO_{x(g)} \uparrow .$$

Cell/device characterization.— Typical solar cells have a conventional SLG/Mo/absorber layer/CdS/i-ZnO/n-ZnO/Al structure. Light illuminated current-density voltage (*J-V*) characteristics determined from AAA solar simulator are presented in Fig. 8 for the best cell obtained, yielding a power conversion efficiency of $\eta = 1.75 \pm 0.09\%$ with an open-circuit voltage of $V_{OC} = 0.23$ V, a short-circuit current density of $J_{SC} = 21.72$ mA/cm^2, and fill factor of $FF = 0.34$. The cell had a low fill factor because of high series resistances and low shunt resistance. This is probably due to the fairly thick carbon layer formed during the selenization process when the solvent cannot evaporate through the selenized layer. Defects in the crystalline grain structures and recombination along the grains also contribute to lowering the conversion efficiency.

In general, an absorber layer thinner than a micron is not recommended because it hinders smooth flow of electrons. The absorber layer thickness of our cell is less than a micron (~0.5 μm) yet still yields a conversion efficiency of 1.75%. This suggests significant room for improvement if a thicker absorber layer is spray-coated and/or if the carbon layer is removed or reduced.

Conclusions

We demonstrated, for the first time, production of ESD CIS solar cells and report the conversion efficiency. Despite a low cell conversion efficiency, this ESD method holds promises for practical application by the solar cell industry because of its extremely low material consumption rate. Optimized precursor flowrates, which varied with the thermo-electrical properties of the dissolving solvents, were reported. The effect of substrate temperature on the thin films was also examined. The deposition operating conditions that yielded the most uniform layer was used to produce cells for the post-selenization process. Our cells were completed by adding CdS and ZnO layers onto the $CuInSe_2$ absorber layer. Light-illuminated current-density voltage (*J-V*) characteristics demonstrate a power conversion efficiency of $\eta = 1.75\% \pm 0.09$ with an open-circuit voltage of $V_{OC} = 0.23$ V, a short-circuit current density of $J_{SC} = 21.72$ mA/cm^2, and fill factor of $FF = 0.34$. We note that there is a room for improving the cell conversion efficiency by reducing or removing the carbon layer originating from our highly viscous solvents. Such work is underway and future publications will report our successes in producing carbon-free CIS films.

Acknowledgments

This work was supported by the Center for Inorganic Photovoltaic Materials NRF-2011-0007182 and 2010-0010217 funded by the Korean government (MEST). This research was also supported by the Converging Research Center Program through the Ministry of Education Science and Technology (2010K000969). This research was also supported by the Research Center of Break-through Technology Program through the Korea Institute of Energy Technology Evaluation and Planning (KETEP) funded by the Ministry of Knowledge Economy (2009-3021010030-11-1).

References

1. A. Romeo, M. Terheggen, D. Abou-Ras, D. L. Bätzner, F. J. Haug, M. Kälin, D. Rudmann, and A. N. Tiwari, *Prog. Photovolt: Res. Appl.*, **12**, 93 (2004).
2. D. Mitzi, M. Yuan, W. Liu, A. Kellock, S. Chey, V. Deline, and A. Schrott, *Adv. Mater.*, **20**, 3657 (2008).
3. D. Mitzi, L. Kosbar, C. Murray, M. Copel, and A. Afzali, *Nature*, **428**, 299 (2004).
4. D. Mitzi, M. Copel, and C. Murray, *Adv. Mater.*, **18**, 2448 (2006).
5. D. Milliron, D. Mitzi, M. Copel, and C. Murray, *Chem. Mater.*, **18**, 587 (2006).
6. D. Mitzi, M. Yuan, W. Liu, A. Kellock, S. Chey, L. Gignac, and A. Schrott, *Thin Solid Films*, **517**, 2158 (2009).
7. S. Ahn, C. Kim, J. H. Yun, J. Gwak, S. Jeong, B.-H. Ryu, and K. Yoon, *J. Phys. Chem. C*, **114**, 8108 (2010).
8. C. Eberspacher, C. Fredric, J. Pauls, and K. Serra, *Thin Solid Films*, **387**, 18 (2001).
9. M. Tomar and F. Garcia, *Thin Solid Films*, **90**, 419 (1982).
10. J. Bougnot, S. Duchemin, and M. Savelli, *Solar Cells*, **16**, 221 (1986).
11. P. Raja Ram, R. Thangaraj, and O. P. Agnihotri, *Bull. Mater. Sci.*, **8**, 279 (1986).
12. S. Shirakata, T. Murakami, T. Kariya, and S. Isomura, *Jpn. J. Appl. Phys.*, **35**, 191 (1996).
13. M. G. Panthani, V. Akhavan, B. Goodfellow, J. P. Schmidtke, L. Dunn, A. Dodabalapur, P. F. Barbara, and B. A. Korgel, *J. Am. Chem. Soc.*, **130**, 16770 (2008).
14. M. Fujimoto, T. Kado, W. Takashima, K. Kaneto, and S. Hayase, *J. Electrochem. Soc.*, **153**, A826 (2006).
15. S. Roncallo, J. Painter, M. Cousins, D. Lane, and K. Rogers, *Thin Solid Films*, **516**, 8493 (2008).
16. S. Roncallo, J. D. Painter, M. J. F. Healy, S. A. Ritchie, M. V. Finnis, K. D. Rogers, J. J. Scragg, P. J. Dale, and G. Zoppi, *Thin Solid Films*, **519**, 3544 (2011).
17. J. Mooney and S. Radding, *Annu. Rev. Mater. Sci.*, **12**, 81 (1982).
18. J. Shay, S. Wagner, and H. Kasper, *Appl. Phys. Lett.*, **27**, 89 (1975).
19. C. Bates Jr., K. Nelson, S. Atiq Raza, J. Mooney, J. Recktenwald, L. Macintosh, and R. Lamoreaux, *Thin Solid Films*, **88**, 279 (1982).
20. C. Abernathy, C. Bates Jr., A. Anani, B. Haba, and G. Smestad, *Appl. Phys. Lett.*, **45**, 890 (1984).
21. J. Mooney and R. Lamoreaux, *Solar Cells*, **16**, 211 (1986).
22. N. G. Dhere and R. G. Dhere, *J. Vac. Sci. Technol., A*, **23**, 1208 (2005).
23. J. Rosell-Llompart and J. Fernandez de la Mora, *J. Aerosol Sci.*, **25**, 1093 (1994).
24. H. Yoon, J. H. Woo, Y. M. Ra, S. S. Yoon, H. Y. Kim, S. J. Ahn, J. H. Yun, J. Gwak, K. H. Yoon, and S. C. James, *Aerosol Sci. Technol.*, **45**, 1448 (2011).
25. D.-R. Chen, D. Y. H. Pui, and S. L. Kaufman, *J. Aerosol Sci.*, **26**, 963 (1995).
26. O. Lastow and W. Balachandran, *J. Electrostatics*, **65**, 490 (2007).
27. S. Basak, D.-R. Chen, and P. Biswas, *Chem. Eng. Sci.*, **62**, 1263 (2007).
28. O. P. Agnihotri, P. R. Ram, R. Thangaraj, A. K. Sharma, and A. Raturi, *Thin Solid Films*, **102**, 291 (1983).
29. D. V. K. Sastry and P. J. Reddy, *Thin Solid Films*, **105**, 139 (1983).
30. S. C. Jackson, B. N. Baron, R. E. Rocheleau, and T. W. F. Russell, *AICHE J.*, **33**, 711 (1987).
31. A. Parretta, M. Addonizio, S. Loreti, L. Quercia, and M. Jayaraj, *J. Cryst. Growth*, **183**, 196 (1998).